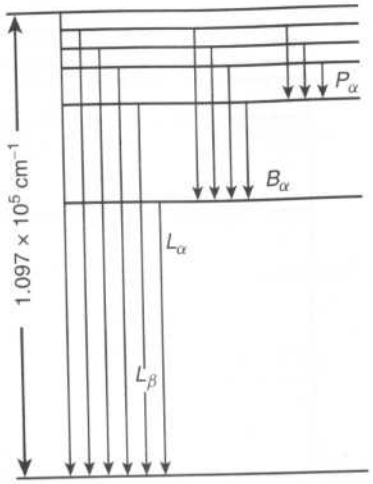

FIGURE 1.13 Transitions between the energy levels of a hydrogen atom. The lines L_α, L_β, etc., belong to the Lyman series, B_α, B_β, etc., to the Balmer series, and P_α, P_β, etc., to the Paschen series, and so forth.

and

$$\frac{1}{\lambda_{if}} = R_\infty \left(\frac{1}{n_f^2} - \frac{1}{n_i^2} \right). \tag{1.15}$$

Indeed, the simple expression of Eq. (1.15) is verified by experiment to a high degree of accuracy.

From Eq. (1.14) (or from Fig. 1.13) we note that the spectral lines of hydrogen will form groups depending on the final state of the transition, and that within these groups many common regularities will exist; for example, in the notation of Fig. 1.13

$$\nu(L_\beta) - \nu(L_\alpha) = \nu(B_\alpha).$$

If $n_f = 1$, then

$$\lambda_{i1} = 91.1 \left(\frac{n_i^2}{n_i^2 - 1} \right) \text{nm} \qquad n_i \geq 2$$

and all lines fall in the far ultraviolet; they form the (so-called) Lyman series. Correspondingly if $n_f = 2$, then

$$\lambda_{i2} = 364.4 \left(\frac{n_i^2}{n_i^2 - 4} \right) \text{nm} \qquad n_i \geq 3$$

and all lines fall in the visible part of the spectrum, forming the Balme series. For $n_f = 3$ the series is named after Paschen and falls in the infrared

1.5. EXPERIMENT ON THE HYDROGEN SPECTRUM

1.5.1. General

To measure the frequency of the radiation emitted by atoms one can us either a grating or a prism to disperse the different wavelengths. Whe using a prism, one exploits the variation, with wavelength, of the refractiv index of certain media. Prism spectrometers are limited to wavelengt regions for which they are able to transmit the radiation; for example in the infrared, special fluoride or sodium chloride prisms and lenses ar used. In the ultraviolet, the optical elements are made of quartz. Also, th sensitivity of the detectors varies with wavelength, so that different type are used in each case (thermopile, photographic emulsion, phototube, etc.

In this laboratory a small constant-deviation prism spectrograph and 2-in. reflection grating spectrometer were used. We will consider in detail measurement of the hydrogen spectrum with the grating, since an absolut value for the wavelengths can be obtained and visual detection is used. A brief discussion of prism spectrographs is given in Section 1.5.4.

From Fig. 1.14, it is evident that the path difference between rays 1 an 2 after reflection is

$$BD - AC = CB \sin\theta_r - CB \sin\theta_i,$$

where CB is the grating spacing d. The angles θ_i and θ_r are both taken a positive when they lie on opposite sides of the normal. Since for constructive interference the path difference must be a multiple of the wavelengt we obtain the condition

$$n\lambda = d\ (\sin\theta_r - \sin\theta_i). \tag{1.16}$$

It can be shown[11] that the resolution of the grating is given by

$$\frac{\lambda}{\Delta\lambda} = nN,$$

where n is the order of diffraction and N the total number of rulings. Th same considerations apply to a transmission grating.

[11] See Chapter 5, Section 5.5.

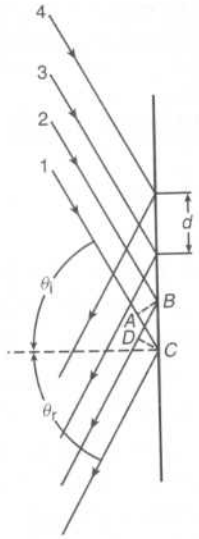

FIGURE 1.14 Schematic diagram of a reflection grating. A parallel beam of radiation is incident along the rays 1 through 4 at an angle θ_i, with respect to the normal; the reflected radiation is observed at an angle θ_r. The spacing between the grooves of the grating is d.

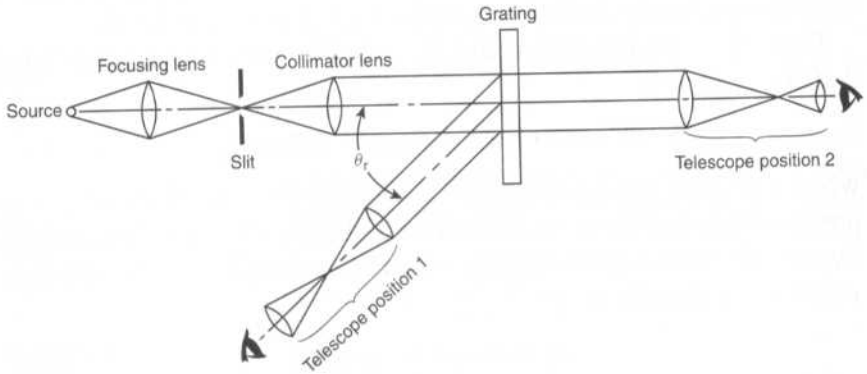

FIGURE 1.15 Diagrammatic arrangement of a grating spectrometer.

The grating is mounted on a goniometer table in the general arrangement shown in Fig. 1.15. A slit and collimating lens are used to form a beam of parallel light from the source, and a telescope mounted on a rotating arm is used for viewing the diffracted lines. It is obviously necessary to ensure

parallelism of the incident and reflected beams, normality of the grating, and so on. A suggested alignment procedure is as follows:

(a) The viewing telescope is focused for parallel rays (on some distant object).

(b) Then with the grating removed, the slit is viewed with the telescope (in position 2) to ascertain that the slit is aligned and in focus; in this way the collimator lens is adjusted.

(c) The source and source lens are placed in position and the alignment and focusing are again checked. The cross hairs are aligned with the slit.

(d) This position of the telescope is carefully noted since it represents the 0° position. The readings on the scale should be made to one minute of a degree by using the vernier and a flashlight.

(e) From now on one may have to work in dark, or by draping the apparatus with a black cloth.

(f) The grating is placed in position and aligned for normal incidence ($\theta_i = 0$). This can be done by "autocollimation"; a strong light is focused onto the slit and a cardboard mask with a narrow slit is placed on the collimator lens. The grating is then adjusted until the reflected image of the cardboard slit coincides with the slit itself.

(g) Finally, the lines of the grating should be made parallel to the slit (hence the cross hairs); this can be done by viewing one edge of the grating with the telescope in position 1.

With any reasonable grating it is possible to observe the visible lines of the spectrum in several orders; thus we expect the measurements for λ/d to be self-consistent, since

$$\sin\theta_{m+1} - \sin\theta_m = (m+1)\frac{\lambda}{d} - m\frac{\lambda}{d} = \frac{\lambda}{d} \tag{1.17}$$

independently of angle of incidence θ_i, or order.[12] The grating spacing d is usually stated by the manufacturer; for example, the grating in this laboratory had rulings on the order of 7000 to the inch ($d = 3.629 \times 10^{-6}$ m). However, d can be obtained by using one or more standard lines of known wavelength.

[12] Provided that both θ_m and θ_{m+1} are taken on the same side of the normal.

The following data were obtained by a student using the grating spectrometer. The source was a low-pressure hydrogen discharge tube (Cenco type 87210) operated at a few thousand volts; a 5-kV transformer and variac were used to provide the variable voltage. The useful life of these discharge tubes is limited because of the appearance of strong molecular bands after some hours of operation.

1.5.2. Determination of d

To obtain the grating spacing d, sodium (Na) was used as a standard, and measurement on three lines (for the shorter wavelength of the doublet) gave the results shown in Table 1.2. Since for all the above measurements θ_i is the same, it follows that

$$d^{-1}(n_k\lambda_k) + \sin\theta_i = \sin\theta_k$$

and a least-squares fit to the linear relation $\beta x + \alpha = y$ can be made; we have

$$\frac{1}{d} = \frac{N\sum(n_k\lambda_k \sin\theta_k) - \sum(\sin\theta_k)\sum(n_k\lambda_k)}{N\sum(n_k\lambda_k)^2 - \left[\sum(n_k\lambda_k)\right]^2}, \tag{1.18}$$

TABLE 1.2 Diffraction Angles from a Sodium Source

λ in nm	Order n	θ_n	$\theta_i = 19°12'$
615.43	1	29°42′	
	2	41°27′	
	3	55°58′	
589.00	1	29°14′	
	2	40°21′	
	3	53°49′	
	4	75°15′	
568.27	2	39°32′	
	3	52°12′	
	4	70°48′	

where the sums are over k, $k = 1, 2, \ldots, N$ and N is the total number of measurements. From the data of Table 1.2 we obtain[13]

$$\frac{1}{d} = 2.7085 \pm 0.009 \times 10^5 \text{ m}^{-1} \tag{1.19}$$

in good agreement with the manufacturer's specification.

Some care must be exercised when comparing wavelengths, since they do depend on the refractive index, n, of the medium in which they are measured,

$$c' = \frac{c(\text{vacuum})}{n},$$

hence

$$\lambda' = \frac{\lambda(\text{vacuum})}{n}.$$

The wavelengths listed in most tables are given for dry air at a pressure of 760 mm mercury. However, any theoretical calculation, such as in Eq. (1.15) predicts the vacuum wavelengths. The refractive index of air at stp is

$$n(\text{air}) = 1.00029. \tag{1.20}$$

1.5.3. The Balmer Series

Measurements on the first four members of the Balmer series, which lie in the visible region, can be made with the spectrometer described above. The data obtained by a student and their reduction are given in Table 1.3.

We observe that the obtained values for the wavelengths of the Balmer series are in agreement with the accepted values at the level of 1/1000. We can now test Eq. (1.15) and obtain the Rydberg wave number. We note that

$$\frac{1}{\lambda} = R_H\left[\frac{1}{4} - \frac{1}{n^2}\right].$$

So that from a least-squares fit

$$R_H = \frac{\sum \rho_i^2}{\sum \lambda_i \rho_i},$$

[13] In reaching this result we have constrained $\theta_i = 19°12'$.

TABLE 1.3 Data on the Balmer Series of Hydrogen as Obtained with a Grating Spectrometer

Color	θ_n	$\sin\theta_n - \sin\theta_i$	Order	Calculated λ	Accepted λ	Balmer series identification
Violet	33°12′	0.22199	2	410.75 ± 6	410.17 H_δ	$n_i = 6$
	41°15′	0.33378	3			
Blue	26°16′	0.11698	1			
	34°06′	0.23483	2	433.82 ± 8	434.05 H_γ	$n_i = 5$
	42°42′	0.35259	3			
Green	27°10′	0.13001	1			
	36°04′	0.26316	2	485.75 ± 10	486.13 H_β	$n_i = 4$
	46°09′	0.39559	3			
Red	30°11′	0.17720	1			
	42°57′	0.35579	2	657.94 ± 14	656.28 H_α	$n_i = 3$
	59°29′	0.53532	3			

Note. All wavelengths are in nm. These measurements used $d = 3692.1 \pm 30$ nm as determined by the previous measurements on the sodium standard lines, and $\sin\theta_i = 0.32557$.

where

$$\rho_i = \frac{4n_i^2}{n_i^2 - 4},$$

giving

$$R_H = (1.09601 \pm 0.003) \times 10^7 \text{ m}^{-1}$$

in good agreement with the accepted value[14]

$$R_H = \frac{M}{M+m} R_\infty = 1.096776 \times 10^7 \text{ m}^{-1}.$$

Here M is the mass of the proton and m the mass of the electron.

1.5.4. The Prism Spectrograph

Long before gratings became widely available, prisms were used as the dispersive element in spectrographs. Prism spectrographs are handy for viewing a large span of the spectrum and come in various ingenious optical

[14]The difference between R_H and R_∞ is due to the motion of the electron about the center of mass rather than about the proton.

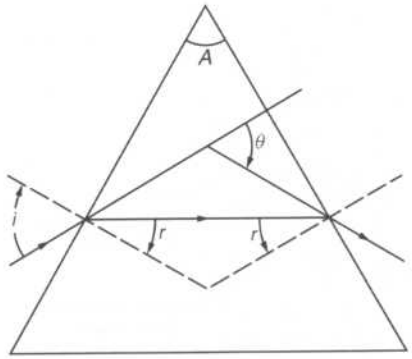

FIGURE 1.16 Diffraction of a ray at minimum deviation through a prism of apex angle A.

arrangements. The dispersion of a prism is a function of the refractive index; thus it cannot be used for absolute measurements without careful calibration.

In the case of a simple prism at minimum deviation (see Fig. 1.16) the diffraction angle θ is given by

$$\frac{\sin\theta_i}{\sin\theta_r} = n \qquad 2\theta_r = A \qquad \theta_i = \theta_r + \frac{1}{2}\theta;$$

thus

$$\sin\left(\frac{A+\theta}{2}\right) = n \sin\frac{A}{2}, \tag{1.21}$$

where θ_i and θ_r are the angles of incidence and refraction, respectively, and A is the apex of the prism. In Fig. 1.17 the refractive index of flint glass as a function of wavelength is given. We note that in the determination of wavelength from the diffraction angle the relation is by no means linear and is in general of serious complexity. Further, most modern prism spectrographs do not consist of a single dispersive element, but of some combination of prisms. The instrument used in this laboratory was of the "constant-deviation" type, and Fig. 1.18 gives the optical paths for an incident ray. It may be seen that the angle of incidence and the angle of exit can remain fixed for all wavelengths by an appropriate rotation of the prism; this has obvious advantages for positioning and alignment of source and detector.

The rotation of the prism is calibrated to give rough wavelength indications, but measurements are made on the exposed photographic plate

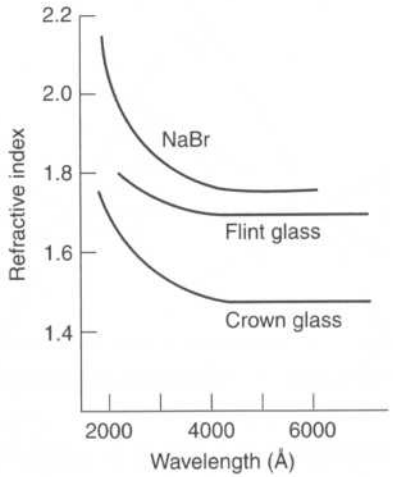

FIGURE 1.17 Refractive index of various materials as a function of wavelength.

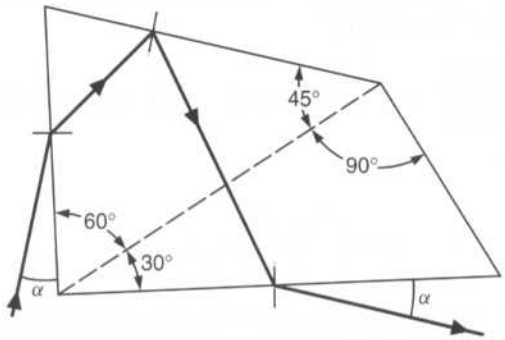

FIGURE 1.18 A constant-deviation prism and the diffraction of a ray passing through it.

or film. A known spectrum is superimposed on the spectrum that is to be investigated, and an interpolation between the known lines is used.

The general arrangement of the spectrograph is shown in Fig. 1.19. Source, lens, and slit should be aligned and the source focused on the slit. By viewing through the eyepiece and varying the prism position, one can get a feeling for the dispersion and the range of the instrument. To obtain photographs of a spectrum, the telescope is replaced by the camera assembly. Several exposures can be had on the same plate; to distinguish different spectra superimposed at the same location on the plate, the "fishtail," which controls the length of the slit, can be used.

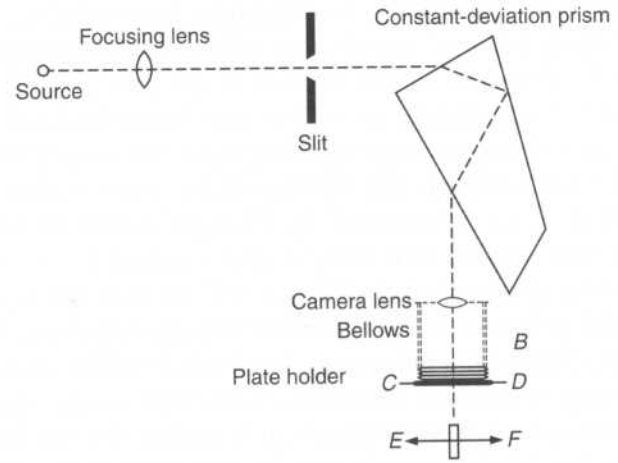

FIGURE 1.19 Schematic arrangement of the constant-deviation spectrograph.

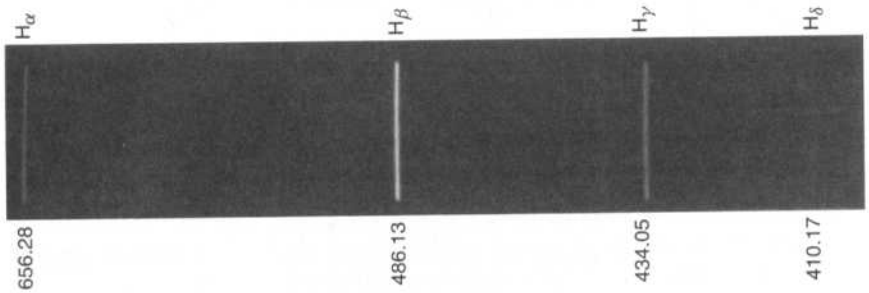

FIGURE 1.20 A spectrogram of the first four lines of the Balmer series of hydrogen as obtained with the constant-deviation spectrograph.

Figure 1.20 shows the first four lines of the Balmer series of hydrogen obtained with the "constant-deviation" spectrograph. A composite exposure containing hydrogen, sodium, and mercury lines is shown in Fig. 1.25.

1.6. THE SPECTRA OF SODIUM AND MERCURY

1.6.1. General

Mention has been made in the previous section of the spectrum of sodium (Na) and mercury (Hg); a brief analysis will be given here, since both

for the "constant" A in terms of the atomic wave function can be found in the references (see Kopferman).

6.3.2. Isotope Shift

Figure 6.9 shows the hyperfine structure of the 253.7-nm line of *natural* mercury when examined under high resolution. When the lines are correctly identified we note that the different isotopes have different energies. Indeed natural mercury consists of several isotopes with the abundances shown in Table 6.3; the nuclear spin, nuclear-dipole magnetic moment, and electric-quadrupole moment are also indicated.

The isotope shift arises from two effects: (a) The finite mass of the nucleus: The nucleus is much heavier than the electron, but we can consider its mass as infinite only to a first approximation. (b) The finite size of the nucleus: The nuclear radius is much smaller than the orbit of the electron, but we can consider the nucleus as a point only to a first-order approximation. For light elements the isotope shift is mainly due to the effect of the finite mass, whereas for the heavy elements it is mainly due to the finite size effect. It should also be evident that we cannot measure the shift in the energy level of a single isotope, but only the difference in the shift between two or more isotopes. This is shown in Fig. 6.10a.

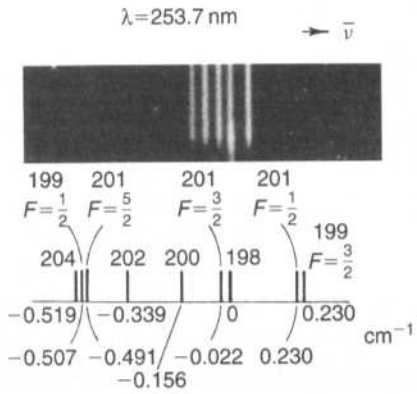

FIGURE 6.9 High-resolution spectrogram of the 253.7-nm line of natural mercury. In the lower part of the figure the various components are identified and their separation from the position of the ^{198}Hg component is also indicated. (Note that the ^{198}Hg component appears in the spectrogram as the longer line.)

TABLE 6.3 Properties of the Isotopes of Natural Hg ($Z = 80$)

Isotope	Abundance (percent)	N (neutrons)	I (nuclear spin)	μ (units of μ_N)	Q ($\text{cm}^2 \times 10^{-24}$)
198	10.1	118	0	0	
199	17.0	119	$\frac{1}{2}$	0.876	
200	23.2	120	0	0	
201	13.2	121	$\frac{3}{2}$	−0.723	0.38
202	29.6	122	0	0	
204	6.7	124	0	0	

In terms of the solutions of the Schrödinger equation we must consider both the electron and nucleus as revolving about the *center of mass* of the electron–nucleus system. This leads back to the Schrödinger equation for a stationary attractive center (nucleus) if the mass of the electron is replaced by its *reduced mass*

$$m' = m_e \frac{M}{M + m_e}, \tag{6.25}$$

where M is the mass of the nucleus. Then the energy of a hydrogen-like level is given by

$$E_n = -\frac{hcR_\infty Z^2}{n^2}\left(\frac{M}{M + m_e}\right) \simeq -\frac{hcR_\infty Z^2}{n^2}\left(1 - \frac{m_e}{M}\right) \tag{6.26}$$

where Z is the nuclear charge. For instance, the value of the Rydberg as obtained from the spectra of hydrogen and deuterium will differ by

$$\frac{R_\text{H}}{R_\text{D}} \simeq \left(1 - \frac{m_e}{2m_p}\right), \tag{6.27}$$

where we set the mass of the deuteron $m_d \sim 2m_p$. This will shift the spectral lines by 3×10^{-4}, which we can observe in the laboratory.

For the heavier elements the isotope shift due to finite mass becomes very small. Instead it is the finite size of the nucleus that is the dominant reason for a shift of the energy levels. Consider Fig. 6.10b where curve (a) represents the Coulomb potential of a point charge. If it is assumed that the electric charge of the nucleus is distributed on a spherical surface of radius r_0, then the potential will not diverge at $r = 0$, but will be constant for all $r \leq r_0$. Thus the potential seen by an electron will be of the form shown

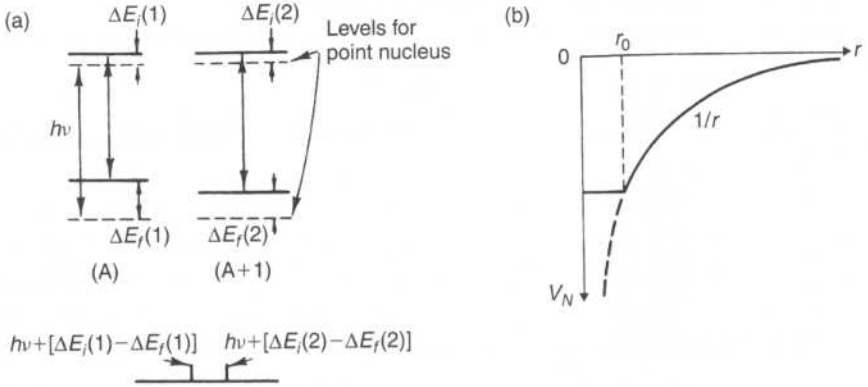

FIGURE 6.10 The isotope shift of atomic spectral lines. (a) The energy levels of the initial and final states of two different isotopes with mass numbers A and $A+1$ are shown. The dashed lines show the position the levels would have if the nucleus was an infinitely heavy point; the solid lines show the actual position of the levels, which are shifted by a different amount for each isotope, and for each level. (b) Modification of the Coulomb potential of the nucleus due to its finite size.

by the solid curve of Fig. 6.10b. This leads to a significant energy shift as a function of r_0. Since the nuclear radius can be expressed as

$$r_0 = A^{1/3} \times 1.2 \times 10^{-13} \text{ cm},$$

where A is the number of nucleons (protons and neutrons) in the nucleus, we see that $\Delta r_0/r_0 = \Delta A/3A$, which can be significant.

6.3.3. Measurement of the H–D Isotope Shift

The hydrogen–deuterium shift is quite large and can be measured with an instrument of modest resolution. The results presented here were obtained with a Jarrell–Ash grating spectrometer. A schematic of the spectrometer is shown in Fig. 6.11 and conforms with the generic spectrometer design introduced in Fig. 5.13. Instead of lenses, focusing mirrors are used to image the entrance slit onto the photomultiplier tube (PMT). The advantage of using a PMT is that very low levels of light can be detected so that the entrance and detector slits can be set to very narrow width. The grating had 630 rulings per millimeter, and the focal length of the lens was $f = 0.5$ m. The spectrum was viewed in second order with a resolution $\Delta\lambda/\lambda \sim 2 \times 10^{-5}$. The angle of the grating was computer controlled so that the speed at which

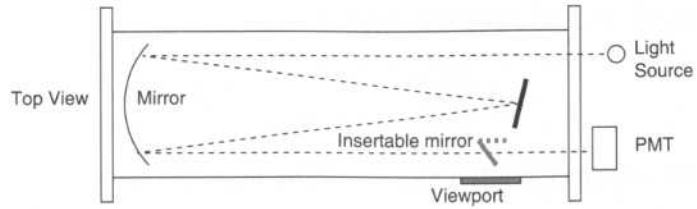

FIGURE 6.11 Schematic layout of the high-resolution Jarrell–Ash grating spectrometer.

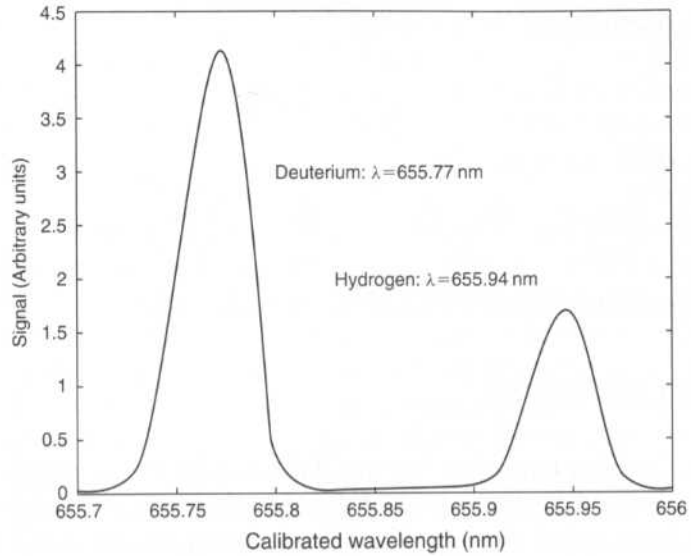

FIGURE 6.12 The red line of the Balmer series for a source containing hydrogen and deuterium observed in high resolution. The absolute wavelength calibration is not exact but this has insignificant effect on the wavelength difference between the two lines.

the spectrum was swept could be adjusted; slow speed for high resolution and vice versa. Furthermore, the grating angle was calibrated to indicate wavelength in nanometers.

For this experiment the source was a discharge tube containing deuterium and an admixture of hydrogen. The entrance slit was closed to a few hundred μm, and the first (red) line of the Balmer series ($n_i = 3$, $n_f = 2$), $\lambda = 656.28$ nm, was examined. The resulting spectrum is shown in Fig. 6.12 where the hydrogen line (longer wavelength) is well separated from the deuterium line. Note that the absolute calibration of the wavelength scale is off by almost 0.3 nm; this is not important in the present case where we are interested in the wavelength difference.

In terms of the calibration we find that

$$\lambda_H = 655.94 \text{ nm}$$
$$\lambda_D = 655.77 \text{ nm}.$$

Convert the wavelength difference into frequency difference

$$\nu_H - \nu_D = c\,\frac{\lambda_D - \lambda_H}{\lambda_D \lambda_H} = -11.85 \text{ GHz},$$

namely, a fractional frequency change

$$\frac{\Delta\nu_{H-D}}{\nu_D} = -\frac{\Delta\lambda}{\lambda} = -2.59 \times 10^{-4}.$$

From Eq. (6.27) we expect that

$$\frac{\Delta\nu_{H-D}}{\nu_D} = \frac{R_H - R_D}{R_D} \simeq -\frac{m_e}{2m_p} = -2.72 \times 10^{-4}$$

in close agreement (within 5%) with the measured value.

6.4. THE LINE WIDTH

Since we are trying to resolve very small differences between the components of a spectral line, it is evident that the width of these components must be narrower than the separation between them. Before the advent of the laser, this was a very difficult task, but today laser lines can be stabilized to a remarkably narrow width, and used for spectroscopic studies.

Spectral lines have a natural width given by

$$\Delta\nu = \frac{\Delta E}{h} \simeq \frac{1}{2\pi\,\Delta\tau}, \tag{6.28}$$

where $\Delta\tau$ is the lifetime of the state; this is usually negligible, since atomic lifetimes are on the order of $\tau \gtrsim 10^{-8}$ s. Thus

$$\Delta\nu \lesssim \frac{1}{2\pi \times 10^{-8}} \sim 15 \text{ MHz}.$$

In wave numbers we find $\Delta\bar{\nu} < 0.05 \text{ m}^{-1}$. However, external influences do broaden spectral lines considerably; the main causes are as follows:

(a) *Doppler Broadening.* Due to their thermal energy, the atoms in the source move in random directions with a velocity given by the Maxwell-Boltzmann distribution. Consequently, the wavelength emitted in a transition of the atom is Doppler-shifted; this results in a broadening of the line, which can be shown to have a half-width

$$\frac{\Delta\nu}{\nu} = 10^{-6}\sqrt{\frac{T}{A}}, \tag{6.29}$$

where T is the absolute temperature in Kelvins, and A is the atomic number of the element. Doppler broadening is most serious for the light elements and in sources that operate at high temperatures. For example, in an arc discharge operating at $T = 3600$ K, a hydrogen line of $\lambda = 500$ nm will have a Doppler width of 36 GHz, which will mask any hyperfine structure. For heavy elements, as in Hg ($A \sim 200$), $\Delta\nu = 3$ GHz, which is still quite broad.

(b) *Pressure (or Collision) Broadening.* When the pressure in the source vapor is too high, the atoms are subject to frequent collisions, which in a way can be thought of as reducing the time interval $\Delta\tau$ entering into Eq. (6.28).

(c) *External Fields.* Magnetic or electric fields produce Zeeman or Stark splitting of the components, resulting in effective broadening of the line. Electric fields of 1000 V/cm can cause a broadening of tens of gigahertz.

(d) *Self-Absorption and Reversal.* This phenomenon is most pronounced with resonance lines. As the radiation emitted from the atoms in the middle of the source travels through the vapor, it has a probability of being absorbed that is proportional to the path length it traverses and to the absorption cross section; this will be strongest in the center of the line and weaker in the wings. The result shown in Fig. 6.13a is that the line becomes "squashed" in the center; that is, it is broadened.

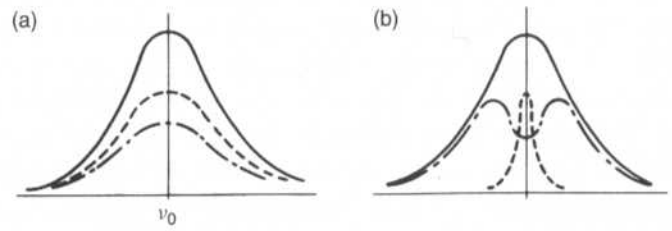

FIGURE 6.13 Broadening of a spectral line due to self-absorption in the source. The solid curve is the emitted line, the dashed curve represents the part of the radiation that is absorbed, and the dash–dot curve shows the transmitted line, which is the difference of the two former curves. (a) Normal absorption, and (b) strong absorption especially in the central region leading to self-reversal.

If the outer layers of the source are much cooler than the middle ones, the width of the particular energy level (due to the Doppler effect) is smaller in the outer layers and absorption takes place only at the central frequency with almost none in the wings. The result is a "self-reversed" line as shown in Fig. 6.13b. This effect is very pronounced in the sodium D lines, and when it is viewed with a high-resolution instrument, the line exhibits a doublet structure that is frequently mistaken for hyperfine structure. One can verify the origin of the effect because it varies with the voltage used to excite the source.

6.5. THE ZEEMAN EFFECT OF THE GREEN LINE OF ^{198}Hg

6.5.1. Equipment and Alignment

We now discuss the observation of the Zeeman effect on the $\lambda = 546.1$-nm line of ^{198}Hg. The choice of the green line is due to its predominance in the mercury spectrum, and the ease with which it can be observed. In an external magnetic field, it is split into nine components, as discussed in detail in Section 6.2.2. In the present observations, a polarizer parallel to the magnetic field was used, so that only three of the nine components (the π light) appeared. Furthermore, natural mercury exhibits in the green line a large number of hyperfine structure components, and each of them forms a Zeeman pattern. To avoid a multiplicity of components in one spectral line, a separated isotope of mercury was used as the source. ^{198}Hg is well suited for this purpose since $I = 0$, and therefore it exhibits no hyperfine structure.

The optical system used for this investigation is shown in Fig. 6.14. The Fabry–Perot was crossed in the parallel-beam method with a small constant-deviation spectrograph (see Chapter 1). The etalon and lenses are all mounted on an optical bench to which the spectrograph is rigidly attached. The pair of lenses L_1 forms the light from the source into a parallel beam, while the pair L_2 focuses the Fabry–Perot ring pattern onto the spectrograph slit; the effective focal length of L_2 is 8 cm, and a further magnification of 2 takes place in the spectrograph.

The discharge tube is mounted vertically, as is the spectrograph slit; the slit width was 1 mm. It is clear that in this arrangement not only is the ring pattern focused onto the spectrometer slit but also the image of the source. A sheet of Polaroid film that could be rotated at will was used as a polarizer.

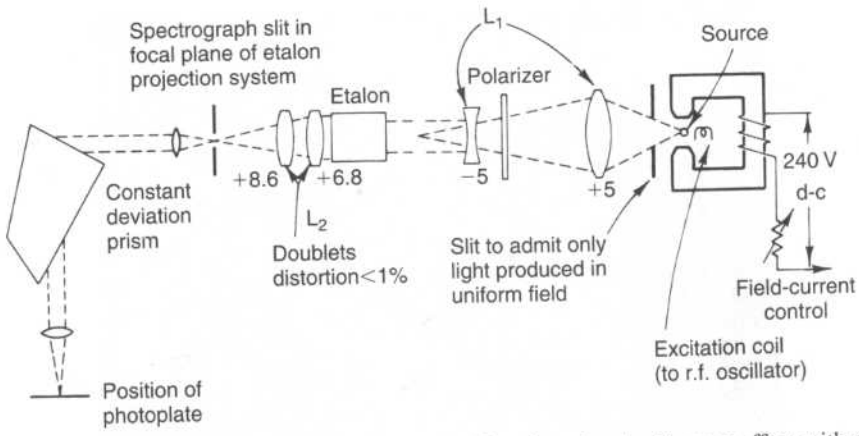

FIGURE 6.14 Experimental arrangement used for observing the Zeeman effect with a Fabry–Perot etalon, crossed by a constant-deviation prism spectrograph.

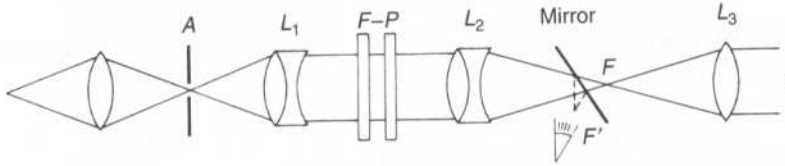

FIGURE 6.15 Optical arrangement for aligning a Fabry–Perot etalon. Rough adjustment is made by viewing the image formed by L_2. Final adjustment is made by viewing the etalon from the point F (or F').

The spacing of the Fabry–Perot etalon is $t = 0.5002$ cm; namely, the free spectral range is FSR = 30 GHz. It is important to adjust the plates carefully for parallelism. This can be done either by viewing through the spectrograph with a frosted glass in the focal plane, and adjusting for the best quality of the pattern, or by a much more sensitive arrangement as shown in Fig. 6.15. A very small aperture (less than 1 mm in diameter) is placed at the position of the source and illuminated with an intense sodium lamp. The Fabry–Perot plates are adjusted to be normal to the optical axis by bringing the image of A reflected by the etalon back onto A. Next, L_3 is adjusted until a series of multiple images of A appears when the observer is located at I; the plates of the etalon can then be roughly adjusted for parallelism by bringing all the images into coincidence. The final adjustment is made by removing L_3 so that the observer locates his eye at F (or a mirror can be used); then fringes of equal width do appear